Journal of Thermal Analysis, Vol. 48 (1997) 1039-1050

DSC STUDY OF $Y_aBa_bCu_cO_{7-\delta}$ HOMOGENEITY IN THE REGION 1050–1300 K

*K. S. Gavrichev, A. V. Khoroshilov, G. D. Nipan and P. Manca**

Kurnakov Institute of General and Inorganic Chemistry, Leninsky prospect, 31, Moscow, 117907, Russia
*Department of Physical Sciences, University of Cagliari, Via Ospedale 72, 09124 Cagliari, Italy

Abstract

Phase transitions of the compositions $Y_{1\pm x}Ba_{2\pm y}Cu_{3\pm z}O_{7-\delta}$ ($x,y=0$–0.2; $z=0$–0.5; step 0.1) were studied by DSC in argon atmosphere in the temperature range 1050–1300 K. The formation of three polymorphous modifications of the 123 phase was observed. The solubilities of yttrium, barium and copper oxides in every modification were determined. The T–x–y phase microdiagram for the 123 phase was mapped out.

Keywords: superconductors, thermal properties

Introduction

Besides the wide dissemination of methods of preparation of $YBa_2Cu_3O_{7-\delta}$ (123)-based HTSC ceramics by solid-state synthesis, the numerous attempts to obtain single-crystal materials by melt technology are continuing. The growth of 123 crystals with defined properties involves some problems, the main ones being (1) the incongruent character of crystallization (melting) and (2) the necessity of oxygen partial pressure control. As the goal of the production of 123 HTSC materials is the preparation of the oxygen-rich *ortho*-phase, the necessity of oxygen pressure control is very important.

The melting (crystallization) process of 123 is accompanied by a phase transition in the system Y_2O_3–BaO–CuO. Most researchers have reduced the analysis of this quaternary system to that of the quasi-ternary systems Y_2O_3–BaO–CuO, $Y_2Cu_2O_5$–$BaCuO_2$–CuO, etc. This simplification influences the results obtained and leads to variations in the isothermal and polythermal joins of the T–x–y phase diagrams of these systems, mapped by different authors [1–9]. Additionally, some authors have attributed the *ortho-tetra* transition only to the oxygen stoichiometry of the 123 phase, suggesting that both modifications have a continuous oxygen homogeneity range [7]. We presumed that at least three polymorphs of 123 exist: two *ortho* and one *tetra*, with the ideal compositions $YBa_2Cu_3O_7$, $Y_2Ba_4Cu_6O_{13}$ ($YBa_2Cu_3O_{6.5}$) and $YBa_2Cu_3O_6$, in which the oxygen content varies insignificantly [10]. Samples with oxygen indices from 6.0 to 6.5 and from 6.5 to 7.0 are two-phase ones for the substances with exact 1:2:3 cation indices, and the oxygen non-stoichiometry of polymorphs is determined by the cation non-stoichiometry.

0368–4466/97/ $ 5.00

John Wiley & Sons Limited
Chichester

DSC studies of samples with compositions $Y_{1\pm x}Ba_{2\pm y}Cu_{3\pm z}O_x$ (x, y=0–0.2; z=0–0.5 with step 0.1) in argon atmosphere in the temperature range 1050–1300 K were carried out in order to corroborate this assumption, and for a precision study of the phase transitions of 123 and determination of the cation solubility up to the incongruent melting temperature.

Experimental

Samples of defined compositions (Table 1) were prepared from Y_2O_3, $BaCO_3$ and CuO (analytical pure-grade) as initial substances by solid-state synthesis. The compositions of the initial substances were checked by mass spectrometry. Prepared samples were identified by X-ray diffraction (DRON–2.0 unit). Superconducting properties were studied by magnetic susceptibility measurements. DTA studies were carried to with a SETARAM DSC-2000 K unit in the scanning regime. A high-purity argon flow atmosphere was applied to prevent the interaction of samples with atmospheric oxygen. Sintered α-Al_2O_3 was used as the reference sample. Samples and reference substance were loaded in alundum crucibles. The sensitivities of the unit were 100 μW (25 μcal s^{-1}) (for power) and 1 μJ (for energy). The high limit of temperature studied was chosen as 1320 K to avoid the interaction of the melt with the crucible material, which gives rise to additional heat effects. Calibration via silver melting showed the precision of the measurements to be ±0.8 K (temperature) or 7.9% (enthalpy) at a scanning rate of 5 K min^{-1}. A higher rate of scanning leads to higher errors, and a lower one to a high probability of chemical reaction of the specimens with the crucible. This latter circumstance induced us to heat samples up to 1120 K at a high rate (20 K min^{-1}) and to stabilize the thermal conditions at 1120 K during 20 min.

The preliminary measurements revealed that the form of the DSC curves and the onset temperature depend on the sample mass. For large masses, some peaks in the

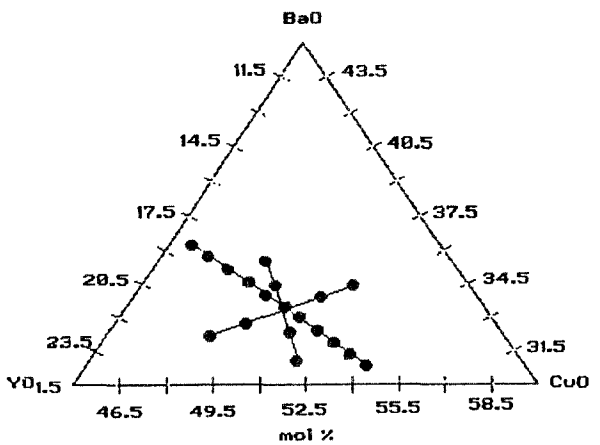

Fig. 1 Positions of studied samples in the concentration triangle of the system $YO_{1.5}$–BaO–CuO. Indices of substance formulas and oxide contents are presented in Table 1

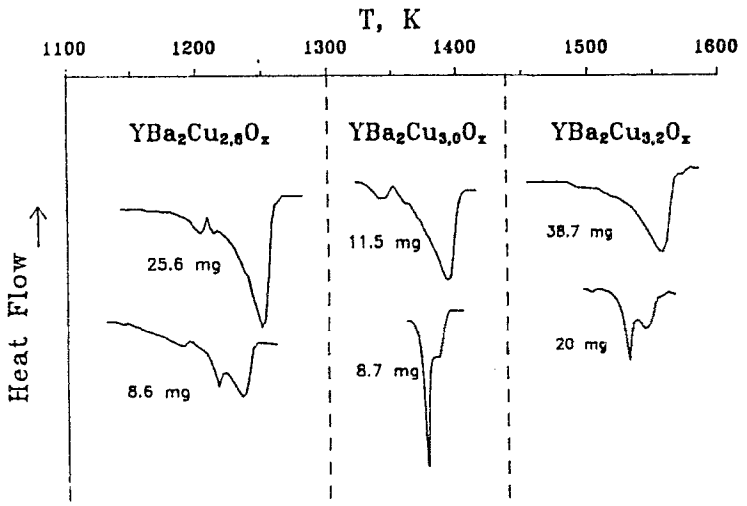

Fig. 2 DTA curves as a function of sample mass

experimental curve were not observed, and another shifted to higher temperatures. At small sample mass, the results of measurements were not reproducible because of the additional peak splitting, obviously caused by the heat effects in the separate grains of the sample. As can be seen from Fig. 2, the temperature shift can be 20 K at a sample mass ratio of less than 1:2. It is possible that the strong dependence of the phase transition temperature on the sample mass is one of the reasons for the great differences between the literature data, and in particular the melting temperature of $YBa_2Cu_3O_{7-\delta}$, ranging from 1200 to 1500 K [4, 7, 11–20].

A constant mass of 20 mg for all samples was used for unification of the experimental conditions. Samples were weighed with a SETARAM analytical microbalance γ-21N4 (accuracy ±0.1 mg). Because of the interaction of 123 with aerial oxygen and moisture, which leads to the degradation of the superconductor, all measurements were carried out on the as-prepared samples. The period from the final annealing to the placing of the crucibles with the samples in the DSC probe was less than 30 min. Values of heat flow, enthalpy of endothermic effects and temperatures were determined from the DSC curves. Transition enthalpy was calculated by peak integration between two points on the baseline. A check on the correctness of these points was performed by a comparison of the results for straight and curved baseline integration.

With regard to the initial enthalpy error, which increases with temperature increase (up to 15% at 1065 K), and some difficulties in its estimation for the multiplet peaks, we used the relative enthalpies ΔH_d. The reported temperatures are related to the peak maxima, and the correct determination of peak onset temperatures was difficult because of the pre-effects. Heat flow was measured with a temperature step of 2 K. Data treatment was carried out with the SETARAM software and self-made programs.

Table 1 Cation indexes *a*, *b*, *c* and related compositions of $Y_aBa_bCu_cO_x$ (in mol%)

No.	*a*–*b*–*c*	$YO_{1.5}$	BaO	CuO	No.	*a*–*b*–*c*	$YO_{1.5}$	BaO	CuO
1	0.8–2.0–3.0	13.79	34.48	51.72	11	1.0–2.0–2.7	17.54	35.09	47.37
2	0.9–2.0–3.0	15.25	33.9	50.85	12	1.0–2.0–2.8	17.24	34.48	48.28
3	1.1–2.0–3.0	18.03	32.79	49.18	13	1.0–2.0–2.9	16.95	33.9	49.15
4	1.2–2.0–3.0	19.36	32.26	48.39	14	1.0–2.0–3.0	16.67	33.33	50
5	1.0–1.8–3.0	17.24	31.03	51.72	15	1.0–2.0–3.1	16.39	32.79	50.82
6	1.0–1.9–3.0	16.95	32.2	50.85	16	1.0–2.0–3.2	16.13	32.36	51.53
7	1.0–2.1–3.0	16.39	34.43	49.18	17	1.0–2.0–3.3	15.87	31.75	52.38
8	1.0–2.2–3.0	16.13	35.48	48.39	18	1.0–2.0–3.4	15.63	31.25	53.13
9	1.0–2.0–2.5	18.19	36.38	45.45	19	1.0–2.0–3.5	15.39	30.77	53.85
10	1.0–2.0–2.6	17.88	35.71	46.43					

Results

All samples were conditionally divided into three sets in accordance with the variation of the cation content for the DTA data treatment. Temperatures and heat flows are listed in Table 1.

Samples with Y non-stoichiometry

For these samples, three endotherms are typical, which correspond to the single peak at 1100 K ($\Delta H_d \geq -11$ J g^{-1}) and the double peak with maxima at 1226 and 1243 K (total enthalpy ≈ -200 J g^{-1}). The small event at 1198 K for the sample $Y_{0.8}Ba_2Cu_3O_{7-\delta}$ disappears on increase of the Y content.

The temperature of the clearly expressed left part of the double peak (1226 K) is independent of the Y content, in contrast with the enthalpy, which varies from -103.3 J g^{-1} ($Y_{0.8}Ba_2Cu_3O_{7-\delta}$) to -77 J g^{-1} ($Y_1Ba_2Cu_3O_{7-\delta}$) and then to -124.1 J g^{-1} ($Y_{1.2}Ba_2Cu_3O_{7-\delta}$). The right peak does not have a sharp maximum and its temperature has the higher error (T=1243.7±2.5 K). The peak enthalpies for $Y_{0.8}Ba_2Cu_3O_{7-\delta}$ and $Y_{1.2}Ba_2Cu_3O_{7-\delta}$ are very close: -112.3 and -116.6 J g^{-1}, respectively; that for $Y_{1.2}Ba_2Cu_3O_{7-\delta}$ is somewhat lower: -75 J g^{-1}.

The greatest variation was found for the endothermic peak near 1108 K. For the composition $Y_{0.8}Ba_2Cu_3O_x$, the enthalpy was -12.5 J g^{-1}; for $Y_1Ba_2Cu_3O_{7-\delta}$, it was very small (-7.1 J g^{-1}); and it disappeared for $Y_{1.1}Ba_2Cu_3O_{7-\delta}$. For the last composition, the DSC curve revealed a set of small peaks ($\Delta H_d < -2$ J g^{-1}) at 1109.6, 1153.4, 1168.3, 1178.4 and 1191.6 K. The DSC curve for the sample of $Y_{0.9}Ba_2Cu_3O_{7-\delta}$ displayed an additional peak at 1131.4 K (-10.9 J g^{-1}). For the sample with the maximum Y content in this set, this part of the DSC curve indicated effects at 1118.3 and 1135.3 K (ΔH_d=-2.8 and 16.3 J g^{-1}, respectively).

Samples with Ba non-stoichiometry

As for the samples with Y non-stoichiometry, the compositions situated in the homogeneity range of 123 yielded additional peaks: for the composition $Y_1Ba_{1.8}Cu_3O_{7-\delta}$ at 1185.3 and 1257 K (ΔH_d=-1 and 5.6 J g^{-1}, respectively) and for $Y_1Ba_{2.2}Cu_3O_{7-\delta}$ at 1151.3, 1177 and 1202.4 K (ΔH_d=-16.8, -18.4 and -50.6 J g^{-1}, respectively). In the DSC curves of this series of samples, heat effects were found only for samples with Ba indices of 1.8 and 1.9. The endotherms are at 1109.5 and 1139.4 K (-55.5 and -36.0 J g^{-1}) for $Y_1Ba_{1.8}Cu_3O_{7-\delta}$, they are closer for $Y_1Ba_{1.9}Cu_3O_{7-\delta}$ (1103.2 K (-12.0 J g^{-1}) and 1116.4 K (2.5 J g^{-1})), and they coincide for $Y_1Ba_2Cu_3O_{7-\delta}$ (1106.8 K (-7.1 J g^{-1})).

The largest peak for $Y_1Ba_{1.8}Cu_3O_{7-\delta}$ is at 1221.1 K (-252.3 J g^{-1}), with a small shoulder at 1231.2 K. In the DSC curve for $Y_1Ba_{1.9}Cu_3O_{7-\delta}$, this peak is absent; instead, there is a double peak with maxima at 1129.3 K (-145 J g^{-1}) and 1238.2 K (-28 J g^{-1}). With increase of the Ba content, the temperature and enthalpy of the left peak gradually decrease, to 1220.5 K and 48 J g^{-1} for $Y_1Ba_{2.2}Cu_3O_{7-\delta}$. The temperature and enthalpy of the right peak increase to 1249.4 K and 180 ±15 J g^{-1} for $Y_1Ba_{2.2}Cu_3O_{7-\delta}$.

Samples with Cu non-stoichiometry

For the samples with Cu non-stoichiometry, the range of metal indices was increased, as admixtural effects on the DSC curves were found only for the compositions $Y_1Ba_2Cu_{2.7}O_{7-\delta}$ and $Y_1Ba_2Cu_{3.4}O_{7-\delta}$. It is interesting to note that for the Cu-rich compositions a shoulder of the main peak was observed besides the additional effects, but for Cu-poor compositions such phenomena were not detected. A 'low-temperature' effect was detected in the composition range from $Y_1Ba_2Cu_{2.9}O_{7-\delta}$ (1099.8 K, -8.2 J g^{-1}) to $Y_1Ba_2Cu_{3.2}O_{7-\delta}$, as a single peak. Ist temperature and enthalpy increased to 1105 K and -27.5 J g^{-1}. On further increase of the Cu content, a second peak appeared, whose temperature varied from 1117.9 K ($Y_1Ba_2Cu_{3.3}O_{7-\delta}$) to 1138.7 K ($Y_1Ba_2Cu_{3.5}O_{7-\delta}$), and its enthalpy from -7 to -19.3 J g^{-1}. The enthalpy of the first peak increased to -75.7 J g^{-1} for $Y_1Ba_2Cu_{3.5}O_{7-\delta}$.

At higher temperatures, more complex processes take place, which are reflected in the DSC curves. The sample with composition $Y_1Ba_2Cu_{2.5}O_{7-\delta}$ gave effects at 1212.9 and 1241.8 K (-49.2 and -115.1 J g^{-1}). On increase of the Cu index to 2.7, the first peak became smoother, with widening of the peak base and displacement of the maximum to 1140 K. For the composition $Y_1Ba_2Cu_{2.8}O_{7-\delta}$, this peak was displaced to 1198.3 K and its enthalpy decreased from -43.9 to -28.6 J g^{-1}. For the composition with Cu index 2.9, this peak disappeared. However, for the compositions $Y_1Ba_2Cu_{2.8}O_{7-\delta}$ and $Y_1Ba_2Cu_{2.9}O_{7-\delta}$ new peak appeared (1216.4 K and 20 J g^{-1}); sharply changed parameters were observed for $Y_1Ba_2Cu_3O_{7-\delta}$ (1225.9 K; -77 J g^{-1}) and almost the same parameters were seen up to the composition $Y_1Ba_2Cu_{3.2}O_x$. The temperature of the second peak for $Y_1Ba_2Cu_{2.5}O_{7-\delta}$ remained almost invariable up to the composition $Y_1Ba_2Cu_{3.1}O_{7-\delta}$ (1244 K). Its enthalpy increased from -115.7 J g^{-1} for $Y_1Ba_2Cu_{2.5}O_{7-\delta}$ to -159.7 J g^{-1} for $Y_1Ba_2Cu_{2.8}O_{7-\delta}$, and then decreased to -94 J g^{-1} for $Y_1Ba_2Cu_{3.1}O_{7-\delta}$. A small enthalpy variation was

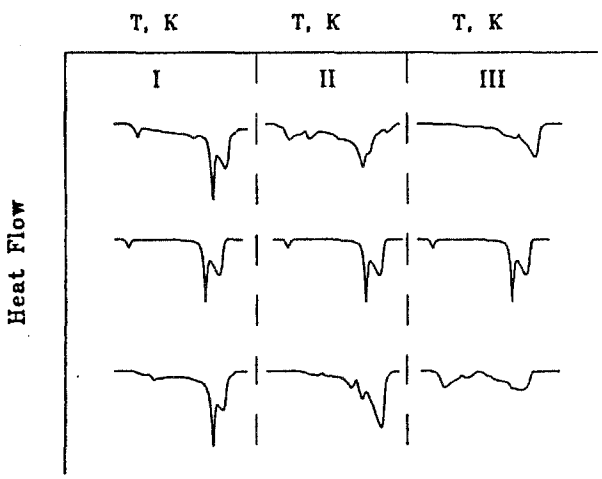

Fig. 3 Variation in DSC curves as a function of cation content in the series
$Y_{0.8}Ba_2Cu_3O_{7-\delta} \rightarrow Y_1Ba_2Cu_3O_{7-\delta} \rightarrow Y_{1.2}Ba_2Cu_3O_{7-\delta}$ (I);
$YBa_{1.8}Cu_3O_{7-\delta} \rightarrow Y_1Ba_2Cu_3O_{7-\delta} \rightarrow YBa_{2.2}Cu_3O_{7-\delta}$ (II);
$YBa_2Cu_{2.5}O_{7-\delta} \rightarrow Y_1Ba_2Cu_3O_{7-\delta} \rightarrow YBa_2Cu_{3.5}O_{7-\delta}$ (III)

found for the peak at 1226 K, from −130.7 ($Y_1Ba_2Cu_{3.2}O_{7-\delta}$) to −153.3 J g^{-1} ($Y_1Ba_2Cu_{3.5}O_{7-\delta}$).

Examples of DSC curve transformations for the samples with limiting deviations from stoichiometry for each cation are shown in Fig. 3. For optimization of the ex-

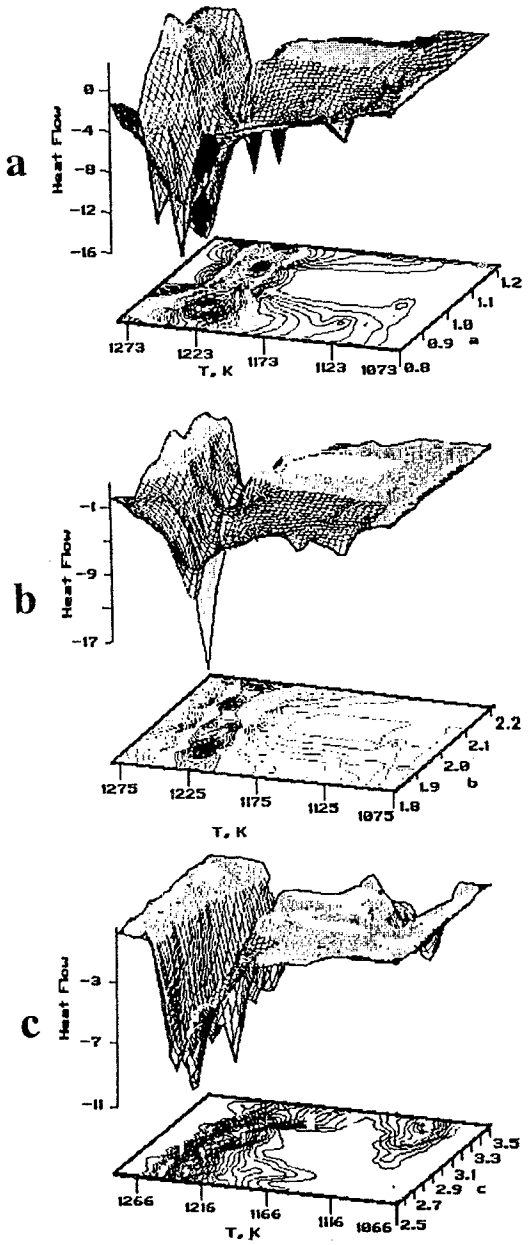

Fig. 4 Phase transition surfaces in the coordinates ΔU–T–x for the studied compositions $Y_aBa_2Cu_3O_{7-\delta}$ (a), $YBa_bCu_3O_{7-\delta}$ (b) and $YBa_2Cu_cO_{7-\delta}$ (c)

perimental data, the heat flow surface of the phase transitions in the three-dimensional space ΔU–T–x were mapped out (where ΔU is the heat flow, T is the temperature in K, and x is the substance composition). The construction was carried out with the Surfer software, which allows a description of the mapped-out surface from every viewpoint and yields its projections on the T–x plane in order to obtain the energy distribution from the temperature and composition for every phase tran-

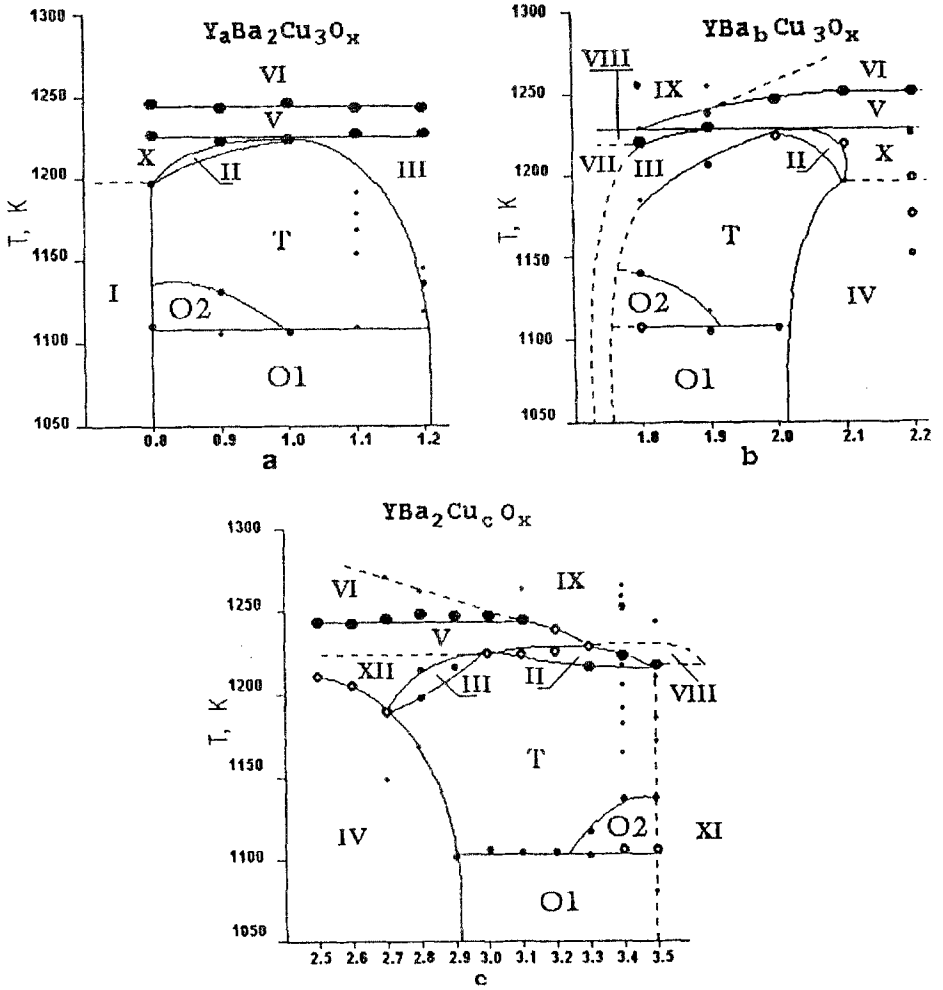

Fig. 5 Polythermic joins of the $Y_aBa_2Cu_3O_{7-\delta}$, $YBa_bCu_3O_{7-\delta}$ and $YBa_2Cu_cO_{7-\delta}$ diagrams. Points correspond to experimental heat effects (• >–90 J g^{-1}; o from –40 to –90 J g^{-1}; • from –5 to –40 J g^{-1}; . <–5 J g^{-1}). Solid lines obtained via sections of volume model (Fig. 6) by planes; dashed lines are the supposed phase boundaries. T, O1 and O2 are the tetragonal and two orthorhombic modifications of $YBa_2Cu_3O_{7-\delta}$, respectively. The following fields were assigned: I–$S_xS_{123}S_{CuO}$; II–$S_{123}L$; III–$S_{123}S_{211}$; IV–S_xS_{123}; V–$S_xS_{211}L$; VI–$S_{011}S_{211}L$; VII–$S_{123}S_{211}S_{CuO}$; VIII–$S_{123}S_{211}L$; IX–$S_{211}L$; X–$S_xS_{123}L$; XI–$S_{123}S_{CuO}$; XII–S_xS_{211} (S_n=solid phase with composition n; L=liquid)

sition. Examples of such surfaces and projections for the studied samples are given in Fig. 4.

As the conditions of the DSC experiments allowed neglect of the partial pressure of oxygen (flow of argon), the T–x projections obtained for the Y, Ba and Cu-series of samples were regarded as fragments of the T–x polythermal joins for the T–x–y diagram of the system Y_2O_3–BaO–CuO. The space modelling of possible phase volumes was used in mapping out the best variant of the T–x–y diagram near the 123 composition, on the basis of the principles of conformity and constancy formulated by Kurnakov [21]. Mapping out was carried out in the volume confined by the sides of the joins (Fig. 5) intersected by the line of stoichiometric cation content 1:2:3 (Fig. 1). Polythermal joins are given in Fig. 5, together with experimental points.

Discussion

The homogeneous volumes of three polymorphs of the 123 phase and heterogeneous volumes corresponding to two- and three-phase equilibria were mapped out in the intercoordination of experimental polythermal and isothermal joins in the T–x–y space for Y_2O_3–BaO–CuO. The polythermal joins of the T–x–y diagram at $-0.2 \leq x \leq +0.2$, $y=0$, $z=0$ (a); $x=0$, $-0.2 \leq y \leq +0.2$, $z=0$ (b); $x=0$, $y=0$, $-0.5 \leq z \leq +0.5$ (c) are shown in Figs 5a –c. The mutual positions of the phase volumes in the T–x–y space are presented in Fig. 6. At the joins, two- and three-phase fields are marked by Roman figures; non-variant horizontal lines are related to four-phase equilibria. For the designation of the phases, the following symbols were used: S=crystal phases, subscript indices show the ideal ratio of cations (the order is the usual Y:Ba:Cu), S_x is the solid solution with cation ratios of from 1:3:2 to 1:6:3), and L is the melt. Concentration fields of polymorphous modification are designated OI (ortho-I), OII (ortho-II) and T (tetra). Figure 5 reveals that the polymorphous transition OI-T or OI-OII (with the following transition OII-T) takes place in the S_{123} phase at 1103 K. The tetra modification of S_{123} melts incongruently at 1223 K and takes part in the non-variant equilibria $S_{123}S_{211}S_{CuO}L$ (1213 K) and $S_{123}S_{211}S_xL$ (1223 K). The third non-variant equilibrium is connected with the peritectic melting (or crystallization) of S_x–$S_{211}S_{011}S_xL$ at 1243 K.

Thus, the detailed study of the S_{123} phase transitions revealed that the melting and crystallization of this phase can not be regarded as the simple peritectic reaction $S_{123}=S_{211}+L$ at 1288 K [4]. An endothermic peak was found at this temperature in our study of stoichiometric samples annealed in an argon flow at 1070 K during 2 h. After such treatment, the samples did not undergo the polymorphous transitions, practically did not dissolve the simple oxides and probably represented the oxygen-impoverished tetragonal modification of S_{123}. The endothermic effects at 1213 and 1223 K are connected not with the isolation of CuO from S_{123} as a result of interaction with CO_2 or with the crucible material in which the synthesis was carried out [22], but with the formation of solid solutions of Y_2O_3, BaO and CuO in $YBa_2Cu_3O_{7-\delta}$. The values of oxide solubility in S_{123} at high temperatures are in agreement with the X-ray diffraction and magnetic susceptibility data on the same

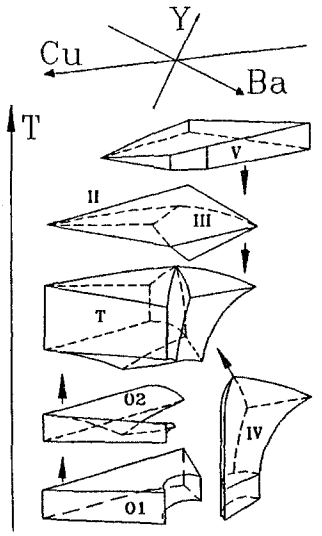

Fig. 6 Three-dimensional model of phase relationships in the system Y_2O_3–BaO–CuO for the region of studied compositions $Y_aBa_bCu_cO_{7-\delta}$

samples at low temperatures [23]. Phase transitions with S_{123} can not be described by using the quasi-binary model (for example 211–123). For this purpose, it is necessary to use at least the three-dimensional diagram.

However, the T–x–y approximation can not be considered the best way of describing phase equilibria with S_{123} as different T–x–y phase diagrams can be obtained at different oxygen partial pressures. This explains the disagreeing polythermal joins presented in a different study [7]. Moreover, in contrast with baria and yttria [24], the copper oxides sublimate and melt incongruently; accordingly, a correct description of the phase equilibria in the Y–Ba–Cu–O (or Y_2O_3–BaO–CuO) system is possible only by using the p–T–x–y–z diagram [25]. The constructions in the x–y–z space of the Gibbs pyramid are necessary for representation of the S_{123} polymorphous modification phase volumes and liquidus surfaces, corresponding to the crystallization of phases in the quaternary system, but this is very complicated.

It is obvious that the solubility of simple oxides in S_{123} is influenced not only by the oxygen partial pressure in high-temperature studies, but also by the partial pressure during the S_{123} synthesis. It was established in our experiments that annealing the same sample in different atmospheres (inert gas, air and an oxygen flow) leads to different phase volume of S_{123} and three different phase diagrams. In the present work, we report the results of studies of samples annealed in air, via DSC, X-ray diffraction and magnetic susceptibility. The preliminary results of investigations of samples annealed in argon and an oxygen flow are as follows:

a) At low oxygen pressure, the solubility of oxides in S_{123} sharply decreases and only one S_{123} polymorphous modification exists (tetragonal).

b) At high oxygen partial pressure (oxygen flow), non-equilibrium states appear and splitting of the S_{123} phase volume (into two parts) takes place.

This result was unexpected, but allows an explanation of some differences in X-ray and magnetic susceptibility data for samples annealed in air and oxygen.

Table 2 Experimental enthalpies and related temperatures from DSC data

a in $Y_aBa_2Cu_3O_x$	T/K	$-\Delta H$/J g^{-1}
0.8	1111–1198–1227–1245	12.5–11.2–103.3–112.3
0.9	1105–1131–1224–1243	3.8–10.9–99.3–116.6
1.0	1106–1226–1246	7.1–77–108.2
1.1	1226–1243	101.1–92.3
1.2	1118–1135–1226–1241	2.8–11.9–124.1–126.2
b in $YBa_bCu_3O_x$		
1.8	1109–1139–1221–1257	55.5–36–252.3–5.6
1.9	1103–1116–1229–1238–1255	12–2.5–145–28–2.2
2.0	1106–1226–1246	7.1–77–108.2
2.1	1221–1249	41.5–166.5
2.2	1151–1177–1203–1220–1249	16.8–18.4–50.6–54.6–195.6
c in $YBa_2Cu_cO_x$		
2.5	1213–1242	49.2–115.1
2.6	1206–1242	42.8–153.2
2.7	1190–1244	43.9–196.2
2.8	1198–1216–1247	28.6–21.9–159.7
2.9	1100–1216–1247	8.2–18.8–130.2
3.0	1106–1226–1246	7.1–77–108.2
3.1	1105–1225–1246	15–65–94
3.2	1105–1226–1240	27.5–136.3–62.8
3.3	1103–1118–1218–1229	26–7–97–62.7
3.4	1107–1137–1224–1252	60.8–6.6–130.7–9.2
3.5	1107–1138–1218	75.7–19.3–153.3

The necessity to standardize the mass of S_{123} samples introduced the specificity in the interpretation of the obtained data. In order to exclude the influence of surface phenomena, connected with the dispersity, the presentation of endothermic effects in the ΔU–T–x space was applied. Such an original treatment of the experimental data is carried out by methods of physico-chemical computer design, using Grapher, Surfer, AutoCad and HP Paintbrush software.

* * *

This work was partially supported by INTAS Grant 93–1707 and an International Science Foundation Grant (MEA000).

References

1 A. A. Bush, V. P. Sirotinkin, Yu. V. Titov and S. E. Mrost, Superconductivity: Phys. Chem. Technol., 2 (1989) 38.
2 G. P. Shveikin, V. A. Gubanov, A. A. Fotiev et al., Electronic Structure and Physicochemical Properties of High Temperature Superconductors, Nauka, Moscow 1990.
3 K. Oka, K. Nakone, I. Masahiro et al., Jpn. J. Appl. Phys., 27 (1988) L1065.
4 T. Aselage and K. Keefer, J. Mater. Res., 3 (1988) 1271.
5 M. Nevriva, E. Pollert, J. Sestak et al., Thermochim. Acta, 127 (1988) 395.
6 F. Holtzberg and C. Feild, Europ. J. Solid State Inorg. Chem., 27 (1990) 107.
7 P. Karen, O. Braaten and A. Kjekshus, Acta Chem. Scand., 46 (1992) 805.
8 McCallym, M. J. Kramer and S. T. Weir, IEEE Trans. Appl. Supercond., 3 (1993) 1147.
9 A. V. Khoroshilov and I. S. Shaplygin, Inorg. Matter., 30 (1994) 579.
10 K. N. Marushkin and G. D. Nipan, Inorg. Matter., 31 (1995) 504.
11 F. Holzberg, P. Strobel and T. K. Worthington, J. Magn. Magn. Mater., 76 (1988) 626.
12 J. Zhang, X. Xiang, J. Huang et al., Supercond. Sci. Technol., 1 (1988) 102.
13 A. Oro and T. Tanaka, Jap. J. Appl. Phys., 26 (1989) L825.
14 J. Takada, H. Kitaguchi, A. Osaka et al., 26 (1987) L1710.
15 R. G. Grebenshchikov, G. A. Mikirticheva, O. G. Shigareva et al., Doklady AN SSSR (Russ.), 302 (1988) 626.
16 V. B. Glushkova, V. A. Krzhizhanovskaya, E. P. Savchenko et al., Doklady AN SSSR (Russ.), 303 (1988) 886.
17 F. Holzberg and C. Field, J. Cryst. Growth, 99 (1990) 915.
18 S. Nomura, H. Yoshino and K. Ando, J. Cryst. Growth, 92 (1988) 682.
19 N. G. Makarova, T. M. Dmitruk, A. N. Nikolaevsky et al., Phys. Low Temp. (Russ.), 17 (1991) 1493.
20 J. Z. Liu, G. W. Grabtree and A. Umezawa, Phys. Lett. A, 121 (1987) 210.
21 N. S. Kurnakov, Selected papers, v.I, AN SSSR, Moscow 1960.
22 T. L. Asselage, Physica C, 233 (1994) 292.
23 T. N. Kol'tsova, G. D. Nipan and Yu. F. Orekhov, Proc. ISSHTS, Hungary, 1995, v. 2.
24 K. N. Marushkin, G. D. Nipan and V. B. Lazarev, J. Chem. Thermodyn., 27 (1995) 465.
25 G. D. Nipan, Inorganic Materials, 30 (1995) 1079.